Cancer Cell
Article

Loss of the Par3 Polarity Protein Promotes Breast Tumorigenesis and Metastasis

Luke Martin McCaffrey,[1,*] JoAnne Montalbano,[2] Constantina Mihai,[1] and Ian G. Macara[3]
[1]Rosalind and Morris Goodman Cancer Research Centre, Department of Oncology, McGill University, Montreal H3A 1A3, Canada
[2]Department of Microbiology, University of Virginia School of Medicine, University of Virginia, Charlottesville, VA 22908, USA
[3]Department of Cell and Developmental Biology, Vanderbilt University Medical Center, Nashville, TN 37232, USA
*Correspondence: luke.mccaffrey@mcgill.ca
http://dx.doi.org/10.1016/j.ccr.2012.10.003

SUMMARY

Loss of epithelial organization is a hallmark of carcinomas, but whether polarity regulates tumor growth and metastasis is poorly understood. To address this issue, we depleted the *Par3* polarity gene by RNAi in combination with oncogenic Notch or Ras^{61L} expression in the murine mammary gland. Par3 silencing dramatically reduced tumor latency in both models and produced invasive and metastatic tumors that retained epithelial marker expression. Par3 depletion was associated with induction of MMP9, destruction of the extracellular matrix, and invasion, all mediated by atypical PKC-dependant JAK/Stat3 activation. Importantly, Par3 expression is significantly reduced in human breast cancers, which correlates with active aPKC and Stat3. These data identify Par3 as a regulator of signaling pathways relevant to invasive breast cancer.

INTRODUCTION

Most solid tumors arise from epithelial cells that have acquired changes in proliferative and organizational capacity. Epithelial cells form characteristic intercellular adhesions and possess apical-basal polarity, which is lost in some invasive and metastatic cancers in a process related to the epithelial-mesenchymal transitions (EMTs) that occur during development (Thiery et al., 2009). However, in many cases, epithelial features are retained. How epithelial tissues establish their organization in a normal state and how this organization is disrupted during cancer progression are still not well understood. In particular, it is largely unknown if the cell polarity machinery is perturbed during tumorigenesis and if such disruptions promote metastasis.

Many of the polarity protein complexes localize to distinct domains within the plasma membrane. The Par genes (Par1, Par3, Par4, Par5, Par6, and atypical PKC [aPKC]) encode an evolutionarily conserved group of polarity proteins that play key roles in many aspects of cell polarization (Goldstein and Macara, 2007). To date and to our knowledge, only Par4, a protein kinase also known as LKB1, has been identified as a tumor suppressor (Jansen et al., 2009), and it remains uncertain if tumorigenesis in patients with mutant LKB1 is caused by loss of its polarity function.

We have focused on Par3, a multidomain scaffolding protein required for the spatial organization of several important signaling proteins (Goldstein and Macara, 2007). Par3 is essential for the delivery of aPKC to the apical surface (Harris and Peifer, 2005; McCaffrey and Macara, 2009), through binding of Par3 to the adaptor protein Par6, which forms a constitutive complex with aPKC. Furthermore, aPKC can interact directly with Par3, which is essential for apical aPKC localization and epithelial organization (Horikoshi et al., 2009; McCaffrey and Macara, 2009). Loss of aPKC from the apical cortex causes spindle pole orientation defects and epithelial mis-organization (Hao et al., 2010). Both the level of aPKC expression and mislocalization correlate with increased invasion and metastasis in breast cancer (Kojima et al., 2008). However, to our knowledge, whether loss of Par3 has a role in regulating aPKC during tumorigenesis is unknown.

Some proteins have oncogenic activity when overexpressed. The Notch receptor, an important transcriptional regulator of stem cell fate, is activated by proteolytic cleavage to release an intracellular domain (NICD), which is found at elevated levels

Significance

Although loss of cell polarity is often considered a hallmark of invasive cancers, there is little experimental evidence for any role of the polarity machinery in tumor suppression. Here, we demonstrate that Par3 polarity protein expression is frequently lost in human breast cancers. In the context of different oncogenes, loss of Par3 increases primary tumor growth and metastatic colonization of the lungs through the production of MMP9 downstream of Jak/Stat3 signaling, which is responsible for the invasive behavior of the tumors. We find that expression of Par3 is anticorrelated with phospho-aPKC, phospho-JAK, phospho-Stat3, and MMP9 expression in human breast cancers, establishing Par3 as a potent tumor growth and invasion suppressor.

in up to 50% of human breast cancers (Pece et al., 2004); and mammary-specific expression of NICD in mice induces breast tumors, though with no metastasis (Hu et al., 2006). Additionally, enhanced growth factor receptor signaling promotes breast cancer. A central effector of growth factor receptor signaling is the Ras oncogene, which, although rarely mutated in breast cancer, is frequently hyperactivated (Clark and Der, 1995). Elevated expression of Neu/ErbB2 or Met receptors is observed in 20%–30% and 15%–20% of breast cancers, respectively, and can inappropriately stimulate Ras-mediated signaling pathways (Reese and Slamon, 1997; Ponzo and Park, 2010).

Progression of in situ breast carcinomas to metastatic disease requires additional steps, and it is now established that inflammation is necessary for this process (Grivennikov and Karin, 2008). Stat3 has a central role in regulating inflammation in breast cancer through a cytokine loop involving IL-6 (Grivennikov and Karin, 2008; Schafer and Brugge, 2007). Stat3 is Tyr phosphorylated by Src or JAK kinases, which induces translocation to the nucleus. Stat3 can be hyperactivated in breast cancers, which promotes invasion and metastasis, although Stat3 activation alone is insufficient to induce tumorigenesis (Barbieri et al., 2010b; Ranger et al., 2009). Therefore, many of the processes that drive tumorigenesis and metastasis are separable, but how they relate to tissue organization is not well understood.

The goal of this study was to determine the role of the apical-basal cell polarity machinery in tumorigenesis, with a focus on the Par3 polarity protein. Using a mouse mammary transplant model coupled with lentiviral transduction, we silenced Par3 expression in the context of two different oncogenes and determined whether loss of Par3 drives tumor growth and/or metastasis. The expression of Par3 was also examined in human breast cancers.

RESULTS

Loss of Par3 Cooperates with NICD to Promote Tumorigenesis

We used lentiviral RNAi to deplete Par3 from primary mammary epithelial cells (MECs) and transplanted them orthotopically into the inguinal (#4) mammary fat pads of syngeneic mice. Previously, we reported that Par3-depleted mammary progenitor cells form disorganized ductal outgrowths that resemble early ductal carcinoma in situ (DCIS) (McCaffrey and Macara, 2009). However, over a period of 24–37 weeks post-transplantation, Par3 depletion did not lead to tumor formation (Figure 1A), suggesting that Par3 is not a classical tumor suppressor. Next, we asked whether loss of Par3 might enhance tumorigenesis in the context of an oncogene. We initially used NICD, which is upregulated in ~50% of human breast cancers (Pece et al., 2004) and drives tumor formation in mice after a latency of ~9 months (Hu et al., 2006). Primary MECs isolated from C3H mice were transduced with lentivirus that expresses active, myc-tagged NICD plus small hairpin RNAs (shRNAs) to either Luciferase (control) or murine Par3, using Par3 shRNA that we had validated previously (McCaffrey and Macara, 2009). We refer to the transduced MECs as NICD/shLuc and NICD/shPar3, respectively. For each animal, 10,000 NICD/shLuc or NICD/shPar3 MECs were injected into contralateral inguinal (#4) fat pads of the same mouse. Immunoblots of tissue lysates showed that myc-NICD was expressed in the tumors and that Par3 silencing was efficient (Figure 1B).

Strikingly, loss of Par3 caused a dramatic reduction in tumor latency for NICD-transduced MECs, with 50% of NICD/shPar3 animals developing tumors by 18 weeks (Figure 1A). We confirmed that tumors were derived from cells expressing both NICD and shPar3 by imaging the GFP marker for the RNAi lentivirus and by staining for myc-NICD (Figures 1C and 1D).

We transplanted NICD/shLuc and NICD/shPar3 MECs into opposite sides of the same mouse, and palpable NICD/shLuc tumors were rarely formed when mice were sacrificed due to the NICD/shPar3 tumor burden. However, in some cases, small NICD/shLuc tumors were found by microscopic examination of the mammary fat pads (Figure 1D). Consistently, all tumors were GFP positive, and tumors derived from NICD/shPar3 MECs were much larger than those from the NICD/shLuc MECs (Figure 1D). Moreover, whereas NICD/shLuc tumors possessed well-defined boundaries, the loss of Par3 induced a more invasive phenotype, with cells protruding into the surrounding fat pad (Figure 1E). Both types of tumors retained epithelial characteristics, including expression of cytokeratin 8, E-cadherin at intercellular junctions and the tight junction marker ZO1 at apicolateral boundaries surrounding microlumens (Figures 1E and 1F). We further examined cellular organization by staining tumor sections for cytokeratin 8 (K8) and cytokeratin 14 (K14). In normal murine mammary ducts, K14 is expressed in myoepithelial cells, whereas K8 is restricted to luminal cells (see Figure S1 available online). Loss of Par3 increased tumor cell heterogeneity in our NICD model (Figures 1E, 1F, and S1). NICD/shLuc tumors were homogeneous and predominantly $K8^{+}K14^{moderate}$, but the NICD/shPar3 tumors displayed a substantially greater degree of cellular diversity.

Loss of Par3 Cooperates with Oncogenic H-Ras to Promote Tumorigenesis

To determine if the promotion of tumor growth by loss of Par3 is specific to NICD or is of more general importance, we asked if Par3 depletion cooperates with a different oncogene, $H\text{-}Ras^{61L}$. Knockdown of Par3 in conjunction with oncogenic GFP-tagged Ras^{61L} significantly reduced tumor latency compared to GFP-Ras^{61L} alone (Figure 2A). Palpable Ras^{61L}/shPar3 tumors had an average latency of 114 ± 68 days compared to Ras^{61L}/shLuc, which had a latency of >230 days. By 37 weeks, 92% of Ras^{61L}/shLuc transplant mice remained tumor-free compared to 54% Ras^{61L}/shPar3 transplant mice (Figure 2A). We confirmed comparable Ras expression levels and efficient Par3 knockdown by immunoblotting tumor lysates (Figure 2B).

Although both Ras^{61L}/shLuc and Ras^{61L}/shPar3 tumors expressed GFP and were able to grow to comparable sizes (Figure 2C), Ras^{61L}/shPar3 tumors grew more rapidly and were consistently more aggressive than Ras^{61L}/shLuc tumors; they invaded through the peritoneum, with the bulk of the tumors growing inside the body cavity, and were not detected during palpation (Figure S2A). Additionally, ~30% of the Ras^{61L}/shPar3 tumors invaded through the skin (data not shown). Consistent with these differences in invasiveness, Ras^{61L}/shLuc tumors were more organized and retained regions that possessed a lobular organization with distinct boundaries, whereas Ras^{61L}/shPar3 tumors exhibited no discernable organization,

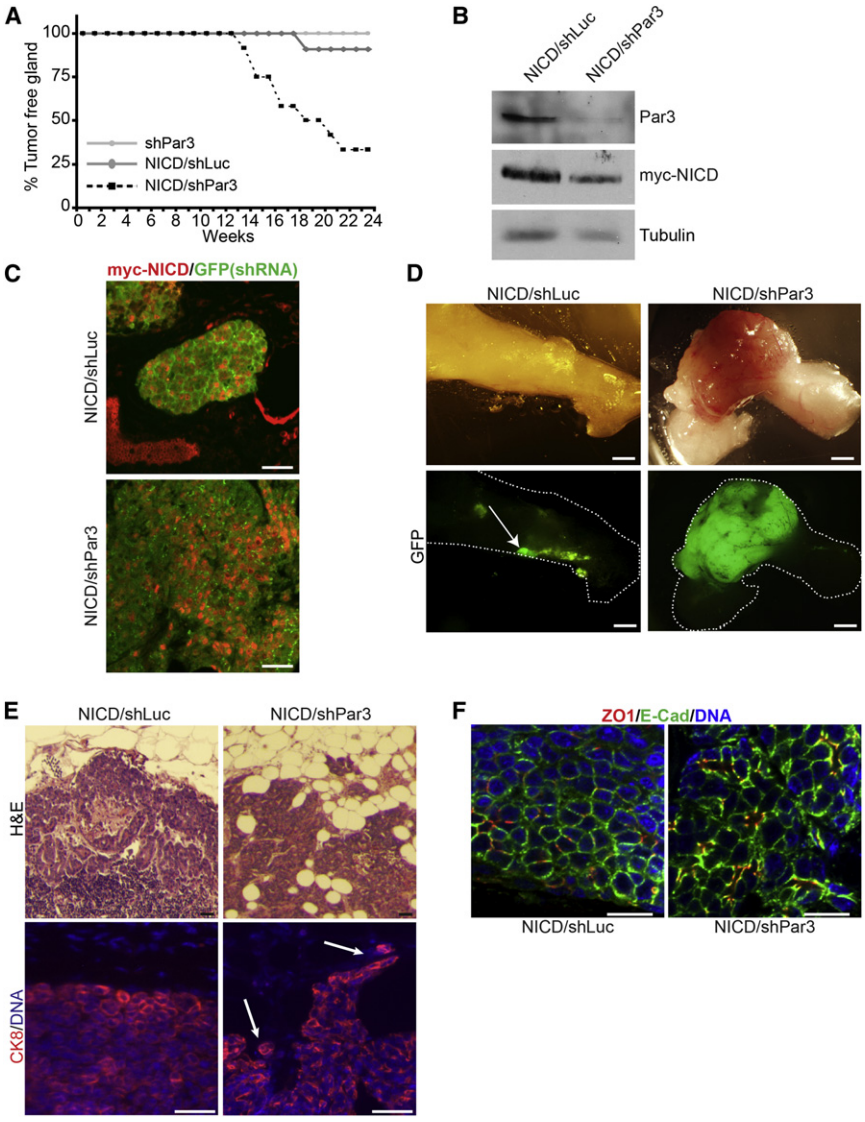

Figure 1. Loss of Par3 Cooperates with NICD to Promote Mammary Tumor Formation

(A) Kaplan-Meier (KM) curve of tumor-free status in mice transplanted with shPar3 (n = 17), NICD/shLuc (n = 11), or NICD/shPar3 (n = 12) MECs.

(B) Tumors arising from orthotopically transplanted myc-NICD/shLuc or myc-NICD/shPar3 MECs were immunoblotted for Par3, myc-NICD, and tubulin.

(C) Immunofluorescence staining of tumor sections for myc-NICD (red) and GFP (green), which marks cells expressing shRNA.

(D) Tumors arising from NICD/shLuc or NICD/shPar3-transduced MECs. GFP is coexpressed with the shRNA and is used as a marker for transduction. Arrow indicates small nonpalpable NICD/shLuc tumors, which were found in 7 of 11 fat pads.

(E) Upper panels show hematoxylin and eosin-stained (H&E) sections of the edges of NICD/shLuc and NICD/shPar3 tumors. Lower panels present tissue sections of the tumor edge stained with CK8 (red) and Hoechst 33258 (DNA, blue). Arrows show invading cells.

(F) Immunofluorescence staining of tumor sections for E-cadherin, ZO1, and Hoechst 33342 for DNA. Scale bars, 50 μm (C), 2 mm (D), 100 μm (E), and 20 μm (F).

See also Figure S1.

and cells appeared more spindle shaped (Figures 2D and 2E). In contrast, NICD/shPar3 tumors were restricted to the fat pad, with occasional invasion into the peritoneum.

Ras tumors depleted of Par3 retained expression of ZO1, which remained localized at sites of cell-cell contacts marking the boundaries of minilumens (Figure 2D). Unexpectedly, although Ras^{61L} is concentrated at intercellular junctions in the Ras^{61L}/shLuc tumors, loss of Par3 results in the partial redistribution of the oncoprotein into the cytoplasm (Figure 2D, insets), which might have consequences for downstream signaling. The tumors also retained expression of the luminal epithelial marker K8 (Figure 2E), demonstrating that, as with the NICD model, the Ras^{61L} tumor cells are disorganized but retain epithelial characteristics in the absence of Par3. The Ras^{61L}/shLuc tumors also expressed E-cadherin (Figure 2E). In contrast, however, E-cadherin (Figure 2E) and β-catenin (Figure S2B) were almost undetectable in Ras^{61L}/shPar3 tumors. The absence of staining reflects downregulation of expression rather than mislocalization (Figures 2F and S2C). Although Ras^{61L}/shPar3 tumor cells were more spindle shaped, there was no increase in vimentin, a mesenchymal marker (Figure 2F). Thus, loss of Par3, specifically in the context of the Ras oncogene, represses E-cadherin expression, though not the loss of other luminal epithelial markers.

Interestingly, Ras^{61L}/shLuc tumor cells were primarily $K8^+K14^-$, whereas the Ras^{61L}/shPar3 tumors were more heterogeneous, and included $K8^+K14^-$ and $K8^+K14^+$ dual-positive cells (Figure 2E). $K8^+K14^+$ dual-positive cells may be undifferentiated progenitors (Raouf et al., 2008; Shackleton et al., 2006; Villadsen et al., 2007). Together, these data are consistent with our previous identification of a role for Par3 in driving progenitor cell differentiation in the mammary gland (McCaffrey and Macara, 2009). They also indicate that loss of Par3 causes tissue mis-organization rather than a simple loss of apical-basal polarity.

Par3 Acts as an Invasion and Metastasis Suppressor

To determine if loss of Par3 promotes metastasis, we examined the lungs of mice after orthotopic injection of NICD/shLuc or NICD/shPar3 into mammary fat pads. None of the NICD/shLuc mice had lung metastases (n = 14), consistent with published data on NICD transgenic mice (Hu et al., 2006). However, >80% of NICD/shPar3 mice (n = 17) displayed extensive colonization, with an average of 32 colonies visible per lung (Figures 3A and 3B). These values are significantly different (p = 0.0001). Importantly, lung metastases from both NICD/shPar3 and

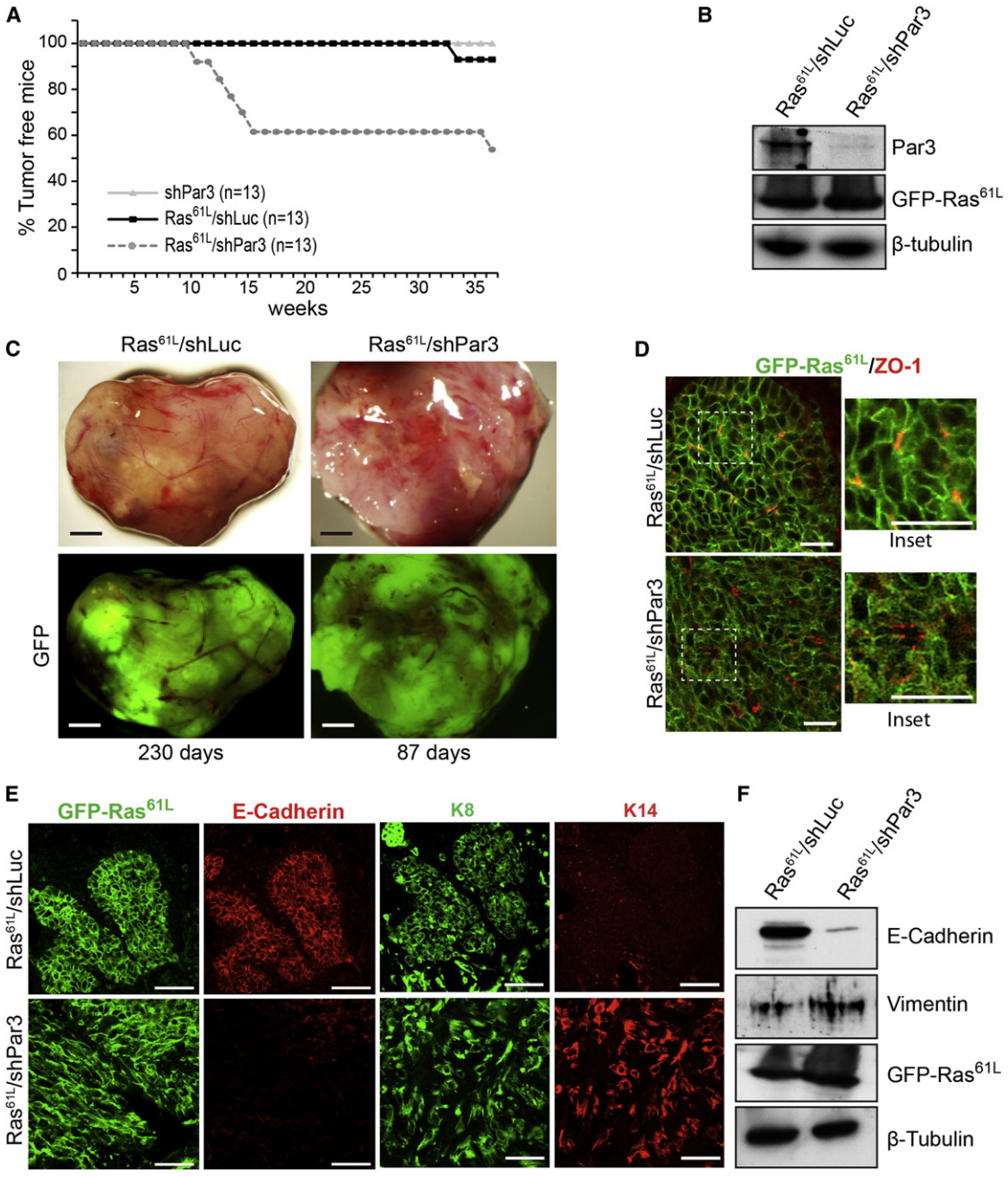

Figure 2. Loss of Par3 Cooperates with Ras^{61L} to Promote Mammary Tumor Formation

(A) KM curve for mice transplanted with MECs expressing GFP/shPar3 (n = 13), Ras^{61L}/shLuc (n = 13), or Ras^{61L}/shPar3 (n = 13).

(B) Immunoblot of primary Ras^{61L}/shLuc and Ras^{61L}/shPar3 tumor lysates.

(C) Micrographs of tumors from transplanted Ras^{61L}/shLuc or Ras^{61L}/shPar3 MECs. GFP indicates tumor cells are transduced with lentivirus.

(D) Immunofluorescence staining of tumor sections for GFP-Ras^{61L} (green) and ZO1 (red).

(E) Immunofluorescence staining of tumor sections for GFP-Ras^{61L} (green) and E-cadherin (red), or CK8 (green) and K14 (red).

(F) Western blot of primary Ras^{61L}/shLuc and Ras^{61L}/shPar3 tumor cell lysates.

Scale bars, 500 μm (C) and 50 μm (D and E).

See also Figure S2.

Ras^{61L}/shPar3 tumors were comprised of similar epithelial cell types as the primary tumors (Figures S3A and S3B). Although Ras^{61L} alone was sufficient to induce metastasis, loss of Par3 increased the number and size of the colonies (Figure S3C).

As a further test of metastatic potential, we injected equal numbers of NICD/shLuc or NICD/shPar3 mammary cells systemically via the tail veins (n = 10), and after 3 weeks, the lungs were sectioned and examined for metastases. In all cases,

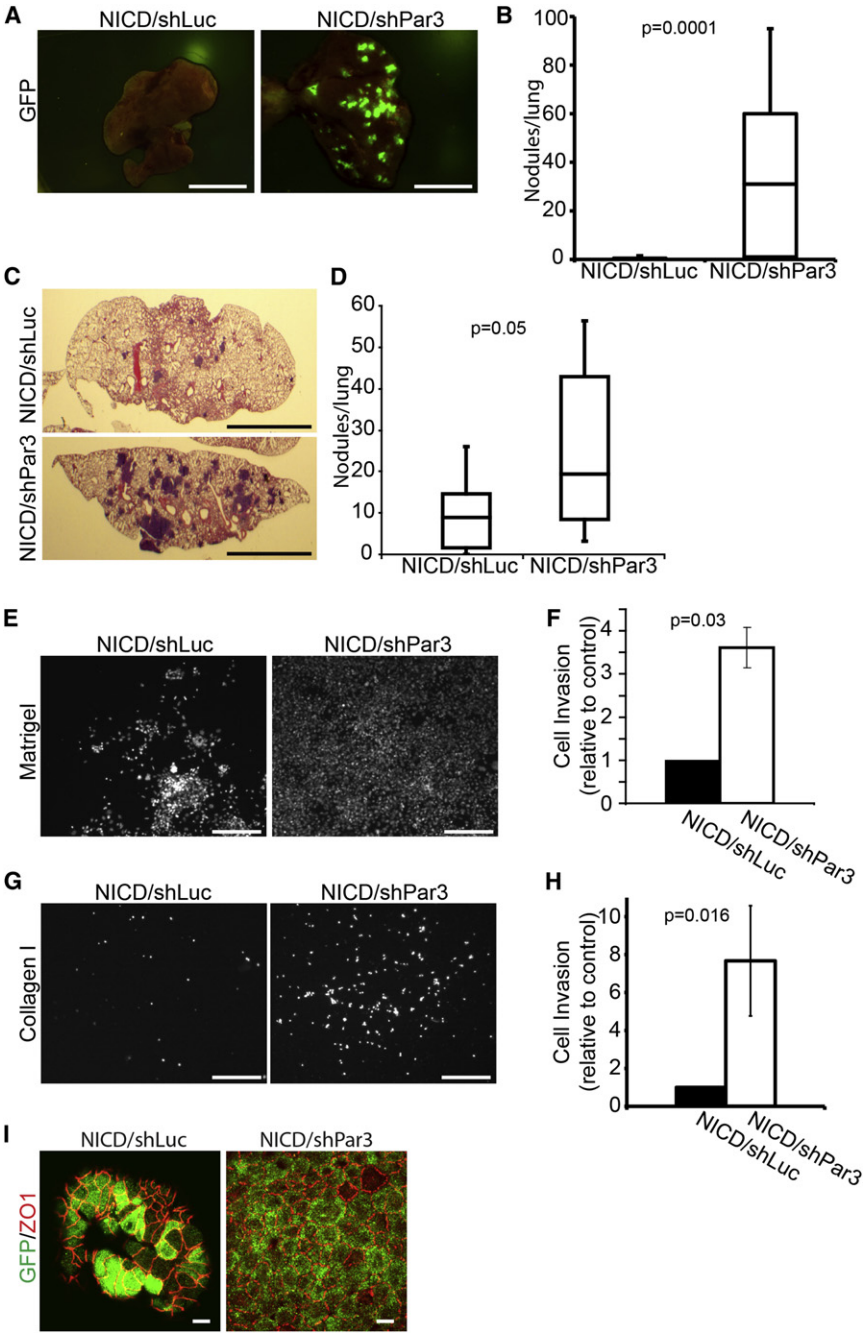

Figure 3. Suppression of Par3 Increases Tumor Invasion and Metastasis

(A) Whole-mount GFP fluorescent images of lung metastases from tumor-bearing mice following orthotopic mammary gland transplants of MECs transduced with NICD/shLuc (n = 14) and NICD/shPar3 (n = 17; p = 0.0001).

(B) Box plots showing the number of metastatic nodules in lungs from (A).

(C) H&E sections of lungs following tail vein injections of 3 × 10^5 MECs transduced with NICD/shLuc or NICD/shPar3.

(D) Box plots showing the number of metastatic nodules in lungs (n = 10) following systemic injections of transduced cells from (C).

(E) Hoechst-stained nuclei of NICD/shLuc or NICD/shPar3 MECs that invaded through the Matrigel pad and 8 μm filter inserts after 72 hr.

(F) Quantification of (E); results are average of three independent experiments. Error bars, 1 SEM.

(G) Same as (E), except invasion through collagen I gels.

(H) Quantification of (G); results are means of three independent experiments. Error bars, SEM.

(I) Immunofluorescence staining of NICD/shLuc or NICD/shPar3 MECs that migrated through the Matrigel for GFP (green) and ZO1 (red).

Scale bars, 1 cm (A and C), 100 μm (E and G), and 10 μm (I).

See also Figure S3.

colonization of the lungs was detected (Figure 3C), but metastases produced by NICD/shPar3 cells were significantly larger and more numerous compared to NICD/shLuc cells (Figure 3D). These results are consistent with increased efficiency of invasion, dissemination, and colonization and support the hypothesis that Par3 normally can suppress metastatic progression.

To further examine the potential for Par3 to suppress tumor invasion, we asked if MECs transduced with or without Par3 shRNA and an oncogene would show increased migration in vitro, using three-dimensional (3D) Matrigel or collagen I invasion assays (Figures 3E–3H, S3D, and S3E). Previously, loss of Par3 has been reported to inhibit cell migration in two-dimensional scratch wound assays (Schmoranzer et al., 2009). The nontransduced cells showed no detectable invasion through Matrigel pads over the time course of the experiment, and silencing of Par3 alone did not enable invasion (data not shown). Expression of either the NICD or Ras^{61L} oncogenes caused a significant number of cells to penetrate through the Matrigel. Strikingly, however, the silencing of Par3 in the context of either oncogene caused a substantial increase in invasion efficiency. Loss of Par3 caused a 3.5-fold (NICD) and 3.9-fold increase (Ras^{61L}) in cells that invaded through the 3D matrix, compared to controls (Figures 3E, 3F, S3D, and S3E). Invasion of NICD cells through collagen I was also stimulated more than 7-fold by loss of Par3 (Figures 3G and 3H).

Although most metastatic carcinomas retain epithelial characteristics, it has been proposed that tumor cells might undergo a transient EMT during dissemination then revert to an epithelial phenotype when they colonize an ectopic site (Guarino et al., 2007). We examined the expression of EMT markers in our cultures and found a modest increase in ZEB1 expression, but no overall changes in gene expression that would indicate a complete EMT (Figure S3F). Interestingly, the NICD/shPar3 cells that had migrated through the matrix to the filter retained

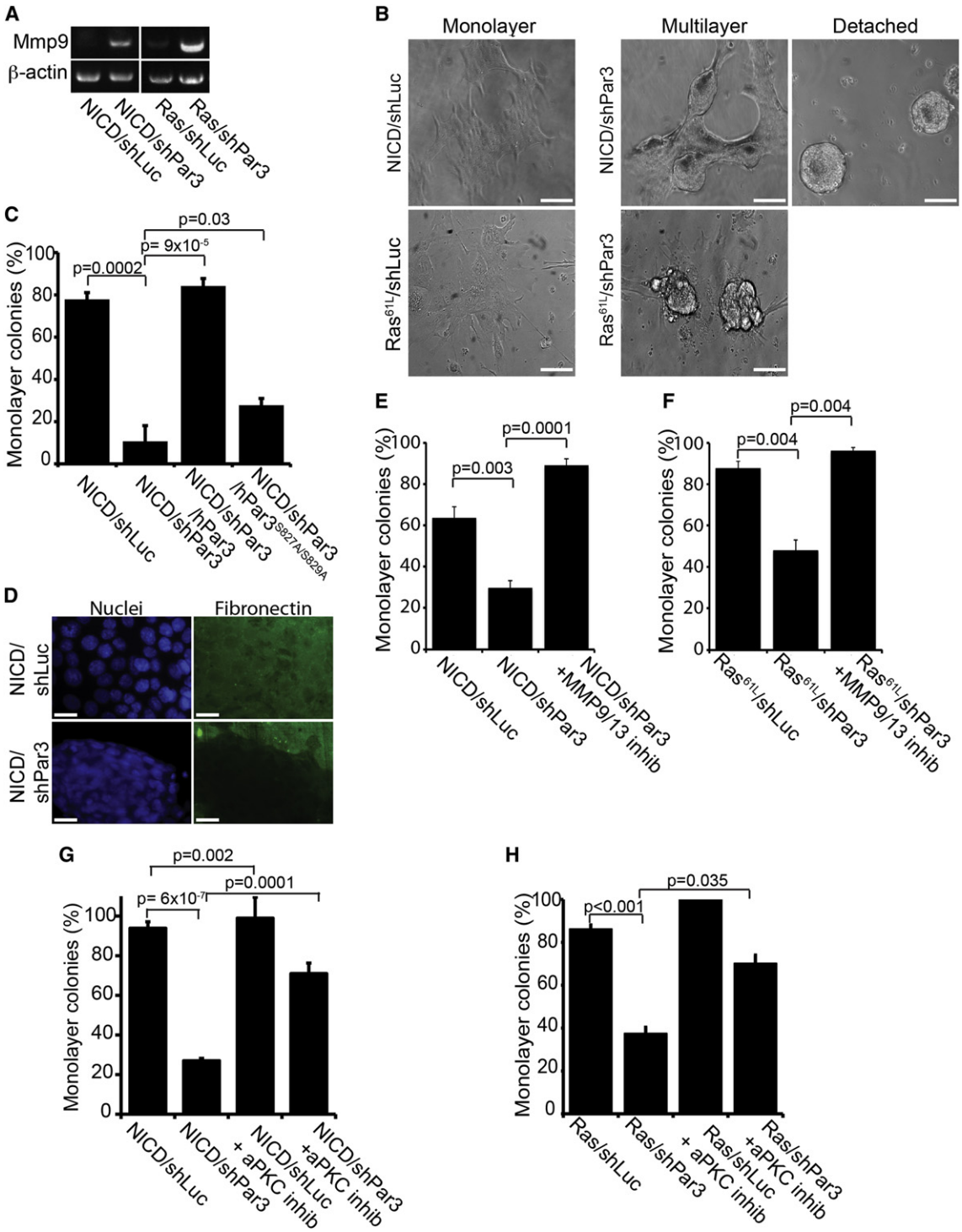

Figure 4. Loss of Par3 Induces MMP Expression and Cell Detachment in Transformed MECs through Activation of aPKC

(A) RT-PCR on total RNA from tumor tissues expressing either NICD or Ras^{61L} with or without shRNA against Par3, using primers for MMP9 and β-actin (control).

(B) Primary MECs stably expressing NICD/shLuc, NICD/shPar3, Ras^{61L}/shLuc, or Ras^{61L}/shPar3 were plated on fibronectin for 72 hr and imaged by DIC. Representative images of the various colony phenotypes are shown. Scale bars, 50 μm.

(C) Quantification of cell detachment by MECs expressing NICD/shLuc, NICD/shPar3, and NICD/shPar3 with RNAi-resistant full-length human Par3, or mutant $Par3^{S827A/S829A}$ that does not bind aPKC.

(D) Immunofluorescent staining of fibronectin under colonies of NICD/shLuc and NICD/shPar3 MECs. Scale bars, 10 μm.

(E) Quantification of cell detachment for NICD/shLuc and NICD/shPar3 MECs with or without 400 pM of MMP inhibitor I.

(F) Quantification of cell detachment for Ras^{61L}/shLuc and Ras^{61L}/shPar3 MECs grown with or without 400 pM MMP9/MMP13 inhibitor I.

expression of the epithelial marker ZO1 (Figure 3I). We conclude that in the context of an activated oncogene, loss of Par3 expression increases invasive behavior, and these cells retain the ability to express epithelial characteristics.

Loss of Par3 Induces MMP Expression and Cell Detachment in Transformed Mammary Cells

Migration through 3D matrices often requires expression of matrix metalloproteinases (MMPs), which degrade the ECM (Rørth, 2009). To test whether loss of Par3, in the context of an oncogene, might alter MMP expression, or expression of other adhesion-related genes, we performed quantitative RT-PCR array analysis of adhesion-related genes on primary NICD/shLuc and NICD/shPar3 MECs in vitro, in the absence of selection. In the context of NICD/shPar3, MMP9 showed the most robust increase in expression over NICD/shLuc, and MMP9 induction was second highest in the Ras model, of all genes analyzed (Tables S1–S4). Changes in MMP9 expression were confirmed by RT-PCR using different primers (Figure 4A). The expression of three other genes was upregulated, and ten genes were reduced in both models (Figure S4A). Expression of other genes differed between the two models, and the expression of some other MMPs was reduced (MMP1a, MMP12, and MMP14 for NICD; and MMP2 and MMP15 for Ras). NICD/shPar3 cells also showed significant decreases in the protease inhibitors, TIMP1 and TIMP2. Therefore, in both models, metalloproteinase expression was altered by Par3 depletion, with MMP9 being the most consistently upregulated gene.

Consistent with induction of MMPs, there was a dramatic change in colony morphology when Par3 expression was suppressed. Most NICD/shLuc cells grew as monolayers on fibronectin-coated dishes (~60%–80%; Figures 4B and 4C). In contrast, only ~10%–30% of NICD/shPar3 cells formed monolayers, with the rest detaching as spheroid colonies after several days' culture (Figure 4B). Importantly, all cultures adhered normally during the first 24–48 hr, demonstrating that maintenance rather than initial adhesive ability of the NICD/shPar3 cells is defective. Moreover, after trypsinization, detached cells were able to readhere to new plates, and again the cells began to detach after 24–48 hr. To determine if loss of Par3 causes defective attachment to specific types of ECM, we also plated cells on collagen I. Whereas ~67% of NICD/shLuc cells grew as monolayer colonies on collagen I, less than 1% of cells lacking Par3 remained as monolayer colonies on collagen I (Figure S4B).

Ras^{61L}-transduced MECs also grew as monolayers, and silencing of Par3 increased multiple layering, whereas detachment occurred as single cells, rather than as multicellular spheroids (Figures 4B, S4C, and S4D). The inability of Ras^{61L}/shPar3 to form spheroids may be due to reduced E-cadherin expression as noted above, which would prevent cells from maintaining intercellular adhesions.

Consistent with the idea that ECM degradation is responsible for cell detachment, staining for fibronectin showed that whereas the ECM was intact beneath cells that express NICD alone, it was absent from patches where clusters of detached NICD/shPar3 cells had formed (Figure 4D). Finally, we asked if MMP activity is required for cell detachment. A MMP inhibitor almost completely blocked detachment induced by Par3 depletion in the context of either NICD or Ras (Figures 4E and 4F). To confirm the involvement of MMP9 in the invasive behavior of the NICD/shPar3 cells, we used shRNA-lentivirus that target the murine MMP9 and transduced them together with the NICD and shPar3 viruses into primary MECs. The two most effective shRNAs (shMMP9-1 and shMMP9-3) significantly reduced invasion through Matrigel (Figures S4E and S4F). The MMP inhibitor also efficiently blocked invasion (Figure S4G). Together, these data identify a mechanism whereby loss of Par3 induces MMP9, which triggers degradation of ECM with consequent cell detachment and increased invasive migration.

Cell Detachment Is Mediated through Inappropriate Activation of aPKC

To confirm that the adhesion defects were caused by loss of Par3, we first performed rescue experiments using shRNA-resistant human Par3, which efficiently restored the ability of cells (85%) to remain attached to the ECM (Figure 4C). Notably, however, a mutant ($Par3^{S827A/S829A}$) that is unable to directly bind and be phosphorylated by aPKC could not rescue the adhesion defects, with only 28% of colonies growing as monolayers (Figure 4C). Next, to determine more directly whether aPKC activity is required for adhesion, we plated cells with or without an aPKC inhibitor. This myristoylated pseudosubstrate peptide penetrates cell membranes and specifically inhibits aPKC isoforms. Inhibition of aPKC completely restored cell-ECM adhesion to NICD/shPar3 and reduced Ras^{61L}/shPar3 multilayering (Figures 4G and 4H).

Our previous work showed that Par3 is required for normal localization of aPKC to the apical surface of luminal epithelial cells (McCaffrey and Macara, 2009). To determine if aPKC is also mislocalized in NICD/shPar3 cells, we stained for aPKC and ZO1. In the NICD/shLuc control, ZO1 and aPKC both formed a tight border around the cells (Figure S4H). Thus, expression of the NICD oncogene alone is not sufficient to disrupt tight junctions and aPKC localization. In contrast, aPKC was completely lost from the apical junctions of Par3-depleted NICD MECs. Cortical ZO1 persisted in Par3-depleted cells but was more punctate (Figure S4H). This result is consistent with our previous studies showing that loss of Par3 negatively affects tight junction formation (Chen and Macara, 2005).

Because inhibiting aPKC can reverse cell detachment, we asked whether aPKC activity was altered in NICD/shPar3 cells. Active aPKC is phosphorylated on T403/T410, and immunoblots of cell lysates for total and p-aPKC revealed a substantial increase in p-$aPKCT^{410}$ levels in NICD/shPar3 cells (Figure 5A, left panels). Thus, in these oncogene-transformed mammary cells, loss of Par3 induces aPKC activation. Notably, however, in normal epithelial cells, although loss of Par3 causes mislocalization of aPKC, it does not alter T410 phosphorylation (Hao et al., 2010).

(G) Quantification of cell detachment for NICD/shLuc and NICD/shPar3 MECs with or without 40 μg/ml of aPKC pseudosubstrate inhibitor.
(H) Detachment of Ras^{61L}/shLuc and Ras^{61L}/shPar3 MECs grown with or without 40 μg/ml aPKC inhibitor.
Results are means of at least three independent cultures. Error bars, ±1 SD.
See also Figure S4 and Tables S1–S4.

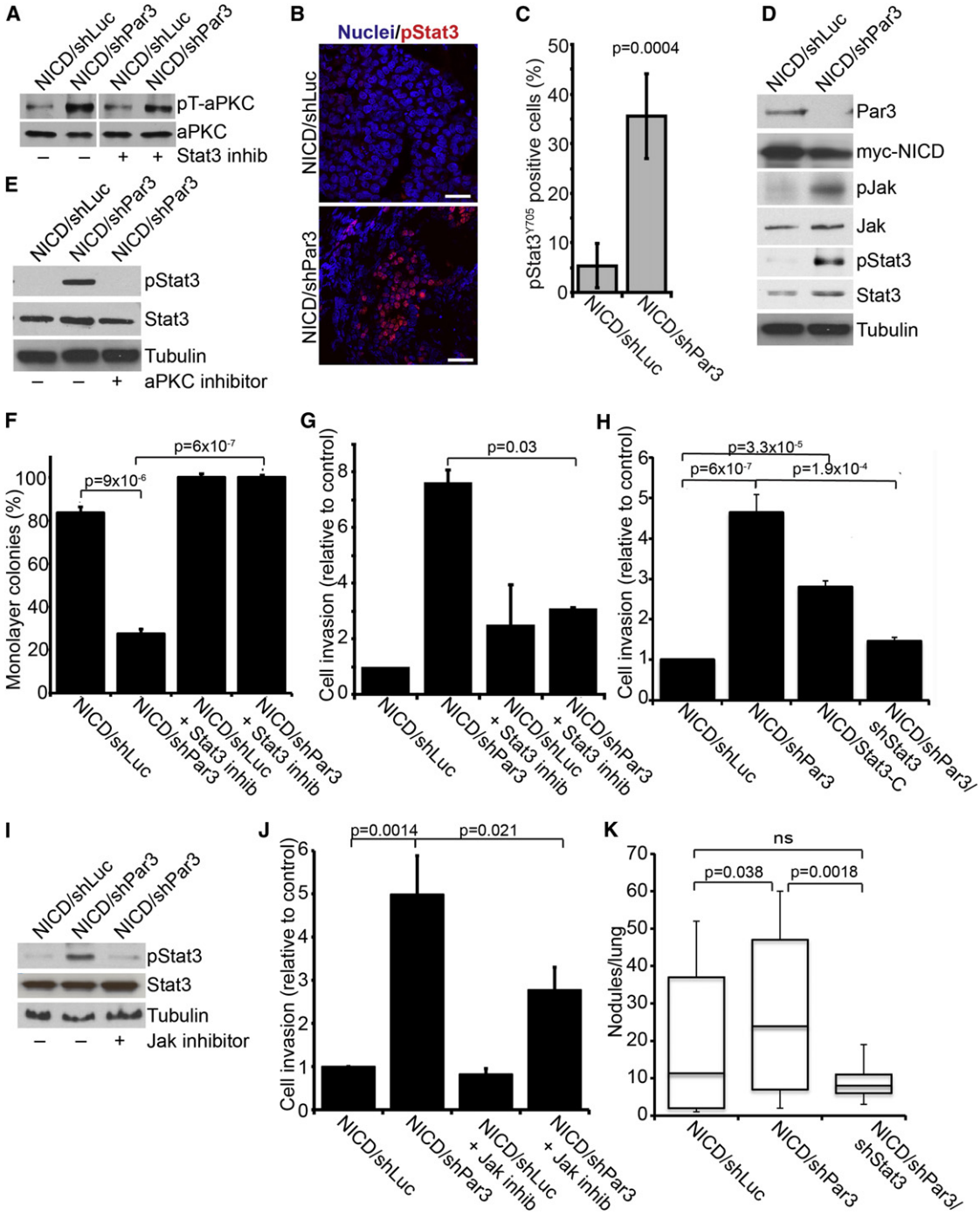

Figure 5. Loss of Par3 Activates Stat3 Signaling through aPKC

(A) Immunoblot of NICD/shLuc and NICD/shPar3 MEC lysates showing active phospho-aPKC$^{T410/403}$ (pT-aPKC) and total aPKC protein levels with or without 50 nM Stat3 inhibitor, Cucurbitacin I.

(B) Immunofluorescence staining of NICD/shLuc or NICD/shPar3 tumor sections for pStat3^{Y705} (red) and nuclei (blue). Scale bars, 50 μm.

(C) Quantification of pStat3^{Y705}-positive cells in tumor sections (n = 8).

(D) Immunoblots of lysates from NICD/shLuc or NICD/shPar3 primary MECs. Phospho-antibodies were used to detect pJAK$^{Y1007/8}$ and pStat3^{Y705}.

(E) Immunoblots of NICD/shLuc or NICD/shPar3 MEC lysates with or without 40 μg/ml aPKC inhibitor.

(F) Quantification of cell detachment for NICD/shLuc and NICD/shPar3 MECs grown with or without 50 nM Cucurbitacin I. Results are from two independent experiments.

(G) Quantification of invasion of NICD/shLuc and NICD/shPar3 MECs through Matrigel with or without 50 nM Cucurbitacin I.

(H) Quantification of invasion of NICD/shLuc, NICD/shPar3, constitutively active Stat3-C, and NICD/shPar3/shStat3 MECs through Matrigel.

(I) Immunoblots of NICD/shLuc or NICD/shPar3 MEC lysates with or without 10 nM JAK inhibitor, Pyridone 6.

Loss of Par3 Activates Stat3 Signaling through aPKC

To determine the mechanism by which Par3 controls adhesion and invasion, we examined potential downstream signaling pathways. Stat3 activation drives MMP expression in multiple cancer cells and promotes invasive behavior (Song et al., 2008; Xie et al., 2004). Active Stat3 is also frequently present at the invasive edge of tumors (Bromberg and Wang, 2009). Therefore, we stained sections from the NICD tumors for phospho-Stat3 (pStat3^{Y705}). Although few cells were pStat3^{Y705} positive in the NICD/shLuc tumors, silencing Par3 increased the number of pStat3^{Y705}-positive cells throughout the tumor mass (Figures 5B and 5C).

In many tumors, Stat3 activation can be induced indirectly through cytokine secretion by infiltrating hematopoietic cells (Yu et al., 2009). To test whether Stat3 activation is intrinsic to NICD/shPar3 epithelial cells, we examined transduced, unselected MECs. Only ~5% of NICD/shLuc cells expressed detectable (but weak) levels of pStat3^{Y705}. Significantly, however, pStat3^{Y705} was present in 18% of NICD/shPar3 MECs, with a higher intensity of staining compared to NICD/shLuc cells (Figures S5A and S5B). Silencing Par3 in Ras^{61L} MECs also caused a substantial increase in pStat3^{Y705}, as judged by immunofluorescence (Figures S5C and S5D). We confirmed that loss of Par3 caused a marked increase in pStat3^{Y705} levels, as determined by immunoblot (Figure 5D). Furthermore, conditioned medium from NICD/shPar3 cultures failed to induce Stat3 activation when added to NICD/shLuc cultures (data not shown). We conclude that Stat3 activation is cell autonomous and does not depend on paracrine cytokine signaling from immune cells.

To determine whether aPKC acts upstream or downstream of Stat3 activation, we inhibited Stat3 and examined aPKC activation by blotting for p-aPKC$^{T403/410}$. aPKC activity was independent of Stat3 activity (Figure 5A). In contrast, treatment of mammary NICD/shPar3 cells with the aPKCps inhibitor diminished pStat3^{Y705} to control levels (Figure 5E), demonstrating that aPKC acts upstream of Stat3 induction.

Because Stat3 can induce MMP expression in some cancer cells, we next tested the effect of a selective Stat3 inhibitor, Cucurbitacin-I (JSI-124), on mammary cell detachment. Cells were treated with 50 nM Cucurbitacin, 24 hr after being plated on ECM, and were examined 48 hr later. Cucurbitacin completely reversed the adhesion defect in NICD/shLuc, NICD/shPar3, Ras^{61L}/shLuc, and in ~80% of Ras^{61L}/shPar3 colonies (Figures 5F and S5E). Moreover, treatment of NICD/shLuc and NICD/shPar3 MECs with Cucurbitacin significantly reduced the invasive potential of the MECs through Matrigel (Figure 5G). In addition, we asked if reducing Stat3 expression could block the effects of Par3 depletion in the invasion of MECs through Matrigel. As shown in Figures 5H and S5F, knockdown of Stat3 significantly reduced the invasiveness of the oncogene-transduced cells that lack Par3. These data suggest that activation of Stat3 is required for the cell detachment and invasive phenotypes caused by loss of Par3.

As a direct test of this hypothesis, we expressed a constitutively active mutant, Stat3-C (Bromberg et al., 1999), in MECs together with NICD or Ras^{61L}. This mutant phenocopied the loss of Par3 by reducing cell attachment and increasing invasion (Figures 5H and S5F). Furthermore, we confirmed that in murine MECs, active Stat3-C also induces MMP9 (Figure S5G).

Jak phosphorylation was also substantially increased by loss of Par3 (Figure 5D). To test whether Jak is upstream of Stat3 activation in Par3-depleted cells, we used a specific Jak inhibitor, Pyridone 6 (Thompson et al., 2002). This inhibitor blocked shPar3-dependent Stat3 activation and significantly reduced invasion of the cells through Matrigel (Figures 5I and 5J).

Importantly, all of the effects on signaling caused by loss of Par3 in the context of oncogenic activation could be fully reversed by expression of a GFP fusion of human Par3 (Figure S5H). GFP-hPar3 did not induce re-expression of the endogenous Par3 but inhibited the phosphorylation of aPKC and Stat3 and blocked the induction of MMP9. Therefore, these signaling responses depend specifically on the loss of Par3 and are not off-target effects of the shRNA.

Finally, to determine whether the induction of Stat3-mediated invasive behavior is significant for shPar3-dependent metastasis in vivo, we measured lung colonization after tail vein injections of NICD-transformed cells with shRNAs against Par3 alone or Par3 and Stat3. As described above (Figure 3), loss of Par3 caused a significant increase in lung metastasis, which was completely suppressed by cosilencing Stat3 (Figure 5K). These data identify an unanticipated pathway in which loss of Par3 results in the aPKC-dependent activation of JAK/STAT signaling, which induces MMP9 expression and consequent destruction of the ECM, increased invasion, and lung metastasis by oncogene-activated mammary cells.

Par3 Expression Is Frequently Lost in Human Breast Cancers

To address the relevance of Par3 loss to human breast cancer, we explored the expression of the *PARD3* transcript in tumors from selected cohorts of patients. Significant reductions in *PARD3* gene expression were apparent in invasive ductal and lobular carcinomas compared to normal breast tissue (Figure 6A). Notably, *PARD3* expression was also reduced in other epithelial cancers (Figure S6A). We next analyzed a human tumor lysate array by immunoblot and found a significant reduction in PAR3 protein for 50% of the tumors as compared to matched samples of normal breast tissue from the same patients (Figure 6Ba). A second, independent matched group of 52 patient samples also showed significant reduction in PAR3 expression (Figure 6Bb). The same membranes were also probed for RanGTPase as a loading control, and the PAR3/RAN ratios were measured, to provide a corrected level of PAR3 (Figure 6C). To validate the specificity of the Par3 antibody, we probed breast cancer cell line lysates under similar buffer conditions to those used in generating the commercial membranes. The antibody

(J) Quantification of invasion of NICD/shLuc and NICD/shPar3 MECs through Matrigel with or without 10 nM Jak inhibitor, Pyridone 6.
(K) Quantification of lung nodules arising from NICD/shLuc, NICD/shPar3, and NICD/shPar3/shStat3-transformed MECs injected systemically. Five sections were examined from each lung of five mice for each treatment. Results are means of at least three independent cultures, unless otherwise noted. Error bars, ±1 SD. ns, not significant.
See also Figure S5.

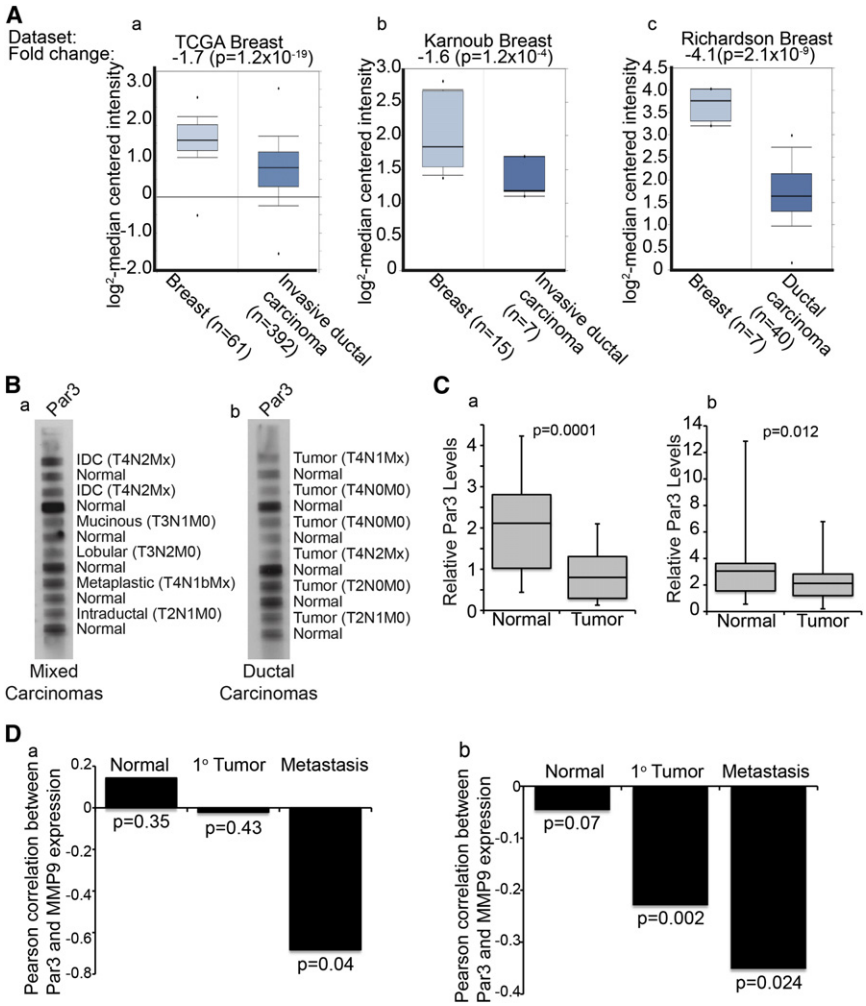

Figure 6. PAR3 Expression Is Reduced in Human Breast Cancer, Correlating with Elevated MMP9 Expression

(A) Microarray data showing relative levels of *PARD3* gene expression for invasive ductal carcinomas versus matched normal breast tissue from TCGA (a), Karnoub (b), and Richardson (c) data sets (see Supplemental Experimental Procedures for information on data sets).

(B) Human tumor protein array membranes of mixed carcinomas (a) and ductal carcinomas (b) with matched normal adjacent tissue were immunoblotted for PAR3. IDC, intraductal carcinoma. TNM classification values are given for each tumor sample.

(C) Box and whisker plots showing quantification of band intensities for PAR3 that were normalized to RAN expression levels in 52 matched human normal and breast tumor lysates from mixed carcinomas (a) and ductal carcinomas (b).

(D) Spearman's correlation coefficients between *PAR3* and *MMP9* expression in normal breast, primary breast tumor, and metastatic human breast cancers from two independent data sets (a, accession number GSE1477; b, accession number GSE7390).

See also Figure S6.

specifically detected PAR3, with low background and no nonspecific bands, indicating that the signal detected on the arrays is PAR3 specific (Figure S6B). In addition, we immunoblotted a limited number of freshly isolated normal and breast tumor samples including three invasive carcinomas (IDC) and one DCIS, which confirmed a decrease in PAR3 protein expression in the invasive breast cancer samples compared to normal tissue (Figure S6C).

To determine if *PARD3* expression is associated with any change in survival probability, we compared Kaplan-Meier plots for high and low expression of *PARD3* using a validated Jetset probe (Figure S6D). For a set of 2,324 patients with breast cancer, low *PARD3* correlated with a modest but statistically significant reduction in survival probability ($p = 9.8 \times 10^{-5}$) (Györffy et al., 2010). Our mouse models had revealed that loss of Par3 triggers the induction of MMP9 and invasion. Therefore, we compared the expression of *PARD3* and *MMP9* in cohorts of normal human breast, primary breast cancers, and metastases. Consistent with a role for loss of PAR3 in regulating metastasis through MMP9, a significant anticorrelation exists between *PARD3* and *MMP9* expression in metastases (Figure 6D). One data set also showed a significant anticorrelation in primary tumors, although to a lesser degree than in metastases (Figure 6Db).

Par3 protein is localized to tight junctions at the apical/lateral boundary in murine mammary epithelia (McCaffrey and Macara, 2009), and immunofluorescence of tissue arrays revealed a similar distribution for human mammary ducts (Figure 7A, a–c). Strikingly, however, PAR3 localization was completely lost in many of the human breast cancer samples (Figure 7A, d–i). From a total of 76 tumor samples examined, 63 lacked strong cortex-associated PAR3 staining. Importantly, costaining of tissue sections of 166 human invasive ductal carcinomas showed that p-aPKC and pSTAT3 were frequently prominent in regions with weak Par3 staining, whereas regions with more intense Par3 staining were negative for $pSTAT3^{Y705}$ and p-aPKC (Figures 7B and 7C). Furthermore, many regions were dual positive for p-aPKC and pJAK2 (Figure 7D), consistent with a role for PAR3 in regulating aPKC, JAK, and STAT3 activity in human breast cancers.

DISCUSSION

The apical-basal polarity of epithelial cells is controlled in part by the Par proteins together with a group of epithelial-specific proteins first identified in *Drosophila* (Crumbs, Scribble [Scrib], Lgl, Dlg). Loss of such proteins, or their misregulation, might therefore be expected to play a pivotal role in carcinogenesis, an idea that has been discussed in numerous reviews (Dow and Humbert, 2007; Feigin and Muthuswamy, 2009; Januschke and Gonzalez, 2008; St Johnston and Ahringer, 2010). Yet, there are surprisingly little published data to support this view. In *Drosophila*, Scrib, Lgl, and Dlg can behave as tumor suppressors

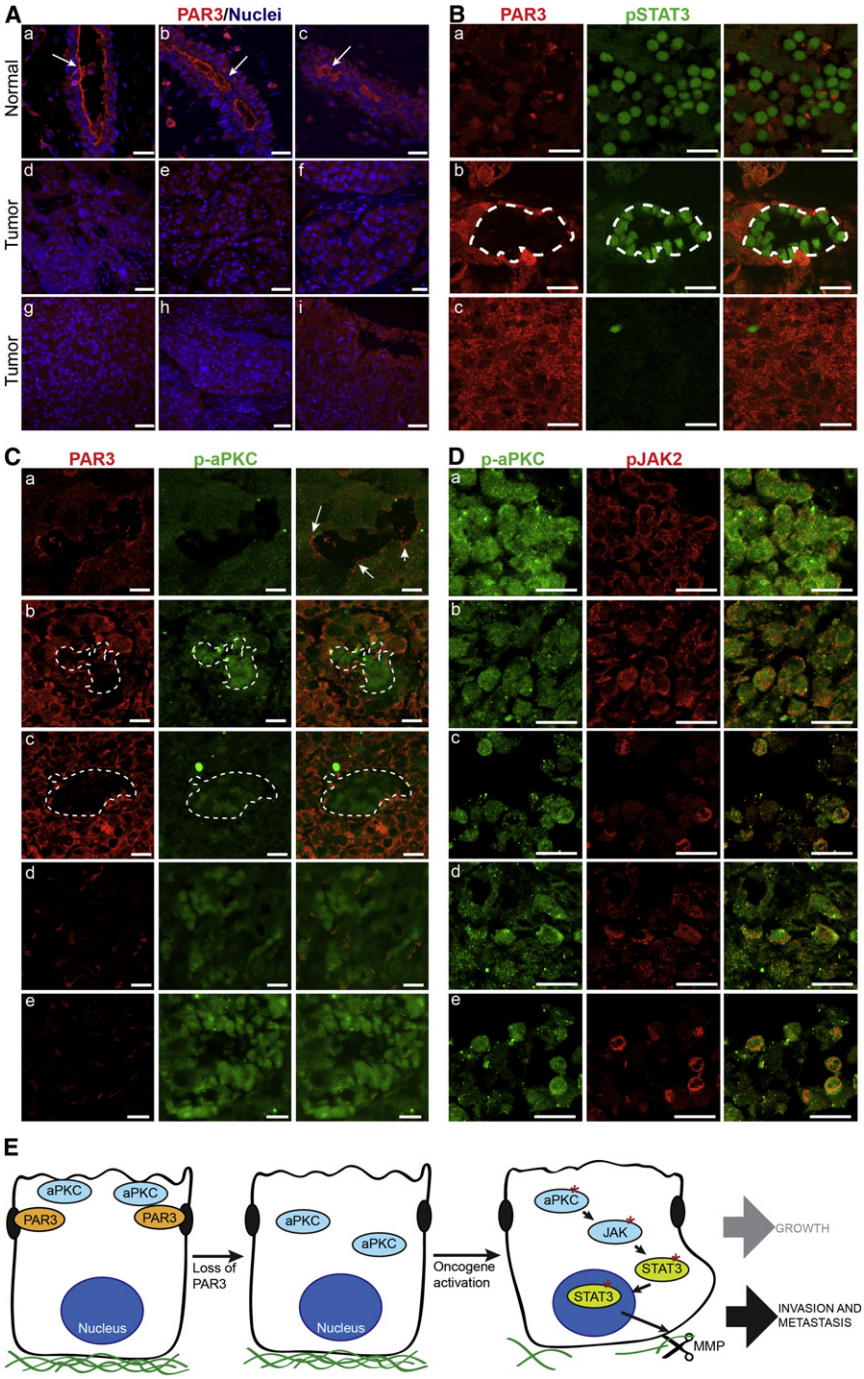

Figure 7. PAR3 Protein Expression Is Reduced and aPKC/STAT3 Signaling Is Activated in Human Breast Cancers

(A) Tissue sections of human normal and breast cancers stained for PAR3 (red) and nuclei (blue). Arrows show PAR3 enriched at the apical membrane. Images represent normal (a–c), infiltrating ductal carcinoma (d–f), and metastatic carcinoma (g–i). Scale bars, 100 μm.

(B) Tissue sections of human invasive breast cancers stained for PAR3 (red) and pSTAT3^{Y705} (green), representative of 166 stained tumor samples. Tumors with weak (top, 64% of tumors), mixed (middle, 28% of tumors), and intense (bottom, 8% of tumors) PAR3 staining.

(C) Tissue sections of human invasive breast cancers stained for PAR3 (red) and active phospho-aPKC^{T560} (green). Arrows show PAR3 enriched at apical membrane and weak p-aPKC staining. Images show representative weak (a, 69% of tumors), mixed (b and c, 25% of tumors), and intense (d and e, 6% of tumors) p-aPKC staining.

(D) Tissue sections of human invasive breast cancers costained for p-aPKC^{T560} (green) and pJAK2$^{Y1007/8}$ (red). Representative images are shown for five tumor samples (a–e).

(E) Model for cooperative effects of loss of Par3 in NICD or Ras^{61L} tumors. Loss of Par3 in the context of either oncogene results in the mislocalization and inappropriate activation of aPKC, which drives the induction and activation of Jak/Stat3 signaling, thereby causing increased MMP expression and ECM degradation.

Scale bars, 30 μm.

(Bilder et al., 2000; Brumby and Richardson, 2003) and can cooperate with oncogenes to drive metastasis (Pagliarini and Xu, 2003; Wu et al., 2010). Deletion of Scrib in prostate epithelium predisposed mice to neoplasia (Pearson et al., 2011). Silencing of Scrib in murine mammary cells stimulated tumor growth driven by c-*myc* but had no effect on tumor latency and did not induce metastasis (Zhan et al., 2008). Nor does silencing of Scrib disrupt apical-basal polarity in mammalian epithelial cells (Dow and Humbert, 2007; Qin et al., 2005). Additionally, increased aPKC activity or Par6 levels have been linked to TGF-β signaling and to breast cancer invasiveness (Viloria-Petit et al., 2009; Zhan et al., 2008). However, to date, and to our knowledge, the only bona fide tumor suppressor among the polarity proteins in humans is PAR4/LKB1 (Jansen et al., 2009), and we are not aware of evidence that other Par proteins function as invasion suppressors or that disruption of a polarity gene can induce tumorigenesis through loss of epithelial polarity.

To examine this issue, we used lentiviruses to deplete Par3 and express activated Notch or Ras in primary murine mammary cells, which were implanted orthotopically into normal immunocompetent mice. An advantage of this approach is that multiple changes in gene expression can be manipulated simultaneously, for instance to couple RNAi with ectopic expression. Additionally, the same cells can be used in vitro, without prior selection, to elucidate the molecular mechanisms underlying their phenotypes. This cancer model revealed several unexpected effects of silencing Par3. Most remarkably, despite the fact that the Ras and NICD oncogenes function through distinct mechanisms, the phenotypes induced by loss of Par3 are very similar. Loss of Par3 potently reduced tumor

latency in both contexts and increased lung colonization, consistent with in vitro increases in invasiveness and detachment from the ECM. These effects were independent of any consistent pattern of EMT. For example, both the NICD and Ras tumors and metastases retained K8 and ZO1 expression and did not express the classical mesenchymal markers vimentin or N-cadherin, consistent with a classification as luminal-type tumors. Moreover, loss of Par3 caused the activation of Stat3 and induction of MMP9 expression in both tumor models. Indeed, the only consistent difference was that Ras/shPar3 tumors had lost expression of E-cadherin, whereas cadherin expression was retained in the context of NICD.

What are the underlying mechanisms through which loss of Par3 triggers rapid tumor growth and invasion? We propose the following model (Figure 7E). First, Par3 spatially restricts aPKC at the apical membrane (McCaffrey and Macara, 2009), and apical localization requires the binding and phosphorylation of Par3 by aPKC. Notably, overexpression or mislocalization of aPKC is commonly found in invasive human breast tumors (Kojima et al., 2008; Regala et al., 2005). Loss of Par3 triggers both the mislocalization and—in the context of at least some oncogenes—the activation of aPKC, which, unexpectedly, triggers JAK-dependent activation of Stat3. Stat3 in turn induces MMP expression, resulting in degradation of the ECM and permitting escape from the primary tumor. Our results generally agree with previous data that aPKCs were necessary for STAT3 activity and MMP1/MMP13 expression in cytokine-stimulated chondrocytes (Litherland et al., 2010). However, Litherland et al. (2010) found a dependence on ERK phosphorylation, whereas we saw no changes in ERK activation in Par3-depleted cells (data not shown). Instead, loss of Par3 in an epithelial tumor context induces Stat3 activation through JAK by a cytokine-independent mechanism.

Stat3 is normally expressed only at low levels in the developing mammary gland and is upregulated during involution to regulate cell death. Nonetheless, active STAT3 is often found at the invasive edges of tumors (Bromberg and Wang, 2009) and is known to promote metastasis in breast cancer (Barbieri et al., 2010a). Brugge and colleagues found that NICD is sufficient to activate STAT3 in MCF10A cells (Mazzone et al., 2010). However, these cells cannot form normal tight junctions and do not exhibit cortical polarity (Fogg et al., 2005). Most likely, therefore, aPKC is not restricted to the apical surface, and NICD expression is sufficient to induce Stat3 activation.

The coupling between polarity proteins, oncogenes, and Stat3 is paralleled to a remarkable degree by *Drosophila*, in which clones of epithelial cells lacking the Scrib polarity protein become highly metastatic in the context of oncogenic Ras (Pagliarini and Xu, 2003; Wu et al., 2010). Loss of Scrib alone triggers a JNK-dependent apoptotic response through the cell competition pathway, by which neighboring wild-type cells eliminate the mutant cells; however, the expression of Ras^{V12} switches this response from apoptosis to uncontrolled proliferation, via a compensatory mechanism dependent on JAK/STAT activation. Tantalizingly, loss of a polarity protein in the mammary gland also stimulates apoptosis, just as in *Drosophila* (McCaffrey and Macara, 2009). An important question for the future is whether this response is mediated by cell competition and whether an aberrant compensatory mechanism drives tumor growth and dissemination when polarity proteins are lost from oncogene-transformed cells.

The striking effects of Par3 deficiency in the context of activated oncogenes suggest that polarity proteins might be suppressors of tumorigenesis in human carcinomas. PAR3 protein levels are significantly reduced in 50% of breast cancer samples compared with matched normal tissue, and a large majority of breast cancers lack normal PAR3 localization. Importantly, loss of Par3 was tightly correlated with increased p-aPKC and pSTAT3 across multiple breast tumor samples. Our data demonstrate that in addition to promoting metastasis through Stat3/MMPs, reduction of Par3 also reduces tumor latency, indicating that Par3 may suppress several steps in tumorigenesis. Microarray data support a broad decrease in *PARD3* gene expression across multiple epithelial cancers, including invasive ductal carcinoma of the breast. Deletions in the *PARD3* locus have also been identified. For human esophageal small-cell carcinoma, the *PARD3* gene was homozygously deleted in 15%, and expression was reduced in 90% of cell lines tested, compared to normal esophageal epithelial cells (Zen et al., 2009). Additionally, small deletions have been identified within the *PARD3* locus in a variety of cancer types (Rothenberg et al., 2010). Because Par3 functions in a polarity signaling network, mutations in other components of this network might also contribute to metastasis by human carcinomas. Together, our data establish that the Par3 polarity protein is an important suppressor of tumorigenesis and metastasis and that it may play a significant role in human breast cancer progression.

EXPERIMENTAL PROCEDURES

Culture Conditions, Antibodies, Immunostaining, and Inhibitors

See Supplemental Experimental Procedures.

Orthotopic Mammary Transplants

All animal procedures were performed in accordance with protocols approved by the Animal Use Committees at the University of Virginia and McGill University, Montreal. Freshly isolated mammary cells were transduced with lentivirus expressing myc-NICD, Ras^{61L}, and control shRNA (shLuc; against luciferase) or shRNA specific to murine Par3 (shPar3) (Zhang and Macara, 2006). Cells were transduced at an moi of 5 for oncogenes and 10 for shRNA. For in vivo tumorigenesis, 1×10^4 transduced MECs for NICD experiments or 1×10^5 MECs for Ras^{61L} were injected into cleared fat pads, as described previously (McCaffrey and Macara, 2009). For assessing tumor incidence and growth, cells expressing NICD/shLuc were injected in the contralateral side to NICD/shPar3 of each mouse. Mice were examined biweekly for palpable tumors. To assess metastasis, cells were transplanted into paired inguinal (#4) fat pads. Once palpable tumors were found, they were measured with calipers weekly. Mice were sacrificed when the calculated tumor volume reached 1 cm^3.

Invasion Assays

A total of 2.5×10^4 primary MECs/well was transduced with NICD/shLuc, or NICD/shPar3, Ras61L/shLuc or Ras61L/shPar3 lentivirus, and 2.5×10^4 Comma-D1 cells/well transduced with Ras^{61L}/shLuc or Ras^{61L}/shPar3 were plated in 8 μm pore Transwell inserts (Corning) in a 24-well plate format on top of 100 μl of 50% growth factor-reduced Matrigel or 100 μl of Collagen I gels (rat tail collagen I; GIBCO), prepared as described by Estecha et al. (2009). Culture medium was changed twice a day for 3 days. After 72 hr, cells that had migrated through the Matrigel to the filter were stained with Hoechst 33342 and counted.

Tumor Array

Commercially available membranes (ST2-6X-1 and ST2-6X-2) and SomaPlex Breast Cancer Tissue Lysate Protein Microarray (PMA2-001-L) from Protein Biotechnologies were probed according to the manufacturer's protocol (see Supplemental Experimental Procedures). Breast tissue was provided by the University of Virginia Biorepository and Tissue Research Facility. All human samples were deidentified and are exempt from informed consent.

Statistical Analyses

A Wilcoxon signed-rank test was used to determine the significance (p value) of tumor-free status in mice for the in vivo tumorigenesis. p Values were determined using unpaired, two-tailed Student's t tests for all assays except the tumor arrays, which used paired two-tailed Student's t tests.

SUPPLEMENTAL INFORMATION

Supplemental Information includes six figures, four tables, and Supplemental Experimental Procedures and can be found with this article online at http://dx.doi.org/10.1016/j.ccr.2012.10.003.

ACKNOWLEDGMENTS

We thank Didier Trono (Lausanne, Switzerland) for lentivectors, Shinya Yamanaka (Kyoto University) for Stat3-C, Connie Cepko (Harvard University) for myc-NICD, Jim Fawcett (Dalhousie University, Canada) for Par3 antibody, and Deborah Lannigan (University of Virginia) for breast tissue samples. We acknowledge support from NIH Grants GM070902 and CA132898 (to I.G.M.) and F32CA139950 (to J.M.), the Terry Fox Research Institute, Project #1009 (to L.M.M.), and CIHR 200602MFE-159430-14-900 (to L.M.M.).

Received: July 8, 2011
Revised: January 5, 2012
Accepted: October 1, 2012
Published: November 12, 2012

REFERENCES

Barbieri, I., Pensa, S., Pannellini, T., Quaglino, E., Maritano, D., Demaria, M., Voster, A., Turkson, J., Cavallo, F., Watson, C.J., et al. (2010a). Constitutively active Stat3 enhances neu-mediated migration and metastasis in mammary tumors via upregulation of Cten. Cancer Res. *70*, 2558–2567.

Barbieri, I., Quaglino, E., Maritano, D., Pannellini, T., Riera, L., Cavallo, F., Forni, G., Musiani, P., Chiarle, R., and Poli, V. (2010b). Stat3 is required for anchorage-independent growth and metastasis but not for mammary tumor development downstream of the ErbB-2 oncogene. Mol. Carcinog. *49*, 114–120.

Bilder, D., Li, M., and Perrimon, N. (2000). Cooperative regulation of cell polarity and growth by *Drosophila* tumor suppressors. Science *289*, 113–116.

Bromberg, J., and Wang, T.C. (2009). Inflammation and cancer: IL-6 and STAT3 complete the link. Cancer Cell *15*, 79–80.

Bromberg, J.F., Wrzeszczynska, M.H., Devgan, G., Zhao, Y., Pestell, R.G., Albanese, C., and Darnell, J.E., Jr. (1999). Stat3 as an oncogene. Cell *98*, 295–303.

Brumby, A.M., and Richardson, H.E. (2003). scribble mutants cooperate with oncogenic Ras or Notch to cause neoplastic overgrowth in *Drosophila*. EMBO J. *22*, 5769–5779.

Chen, X., and Macara, I.G. (2005). Par-3 controls tight junction assembly through the Rac exchange factor Tiam1. Nat. Cell Biol. *7*, 262–269.

Clark, G.J., and Der, C.J. (1995). Aberrant function of the Ras signal transduction pathway in human breast cancer. Breast Cancer Res. Treat. *35*, 133–144.

Dow, L.E., and Humbert, P.O. (2007). Polarity regulators and the control of epithelial architecture, cell migration, and tumorigenesis. Int. Rev. Cytol. *262*, 253–302.

Estecha, A., Sánchez-Martín, L., Puig-Kröger, A., Bartolomé, R.A., Teixidó, J., Samaniego, R., and Sánchez-Mateos, P. (2009). Moesin orchestrates cortical polarity of melanoma tumour cells to initiate 3D invasion. J. Cell Sci. *122*, 3492–3501.

Feigin, M.E., and Muthuswamy, S.K. (2009). Polarity proteins regulate mammalian cell-cell junctions and cancer pathogenesis. Curr. Opin. Cell Biol. *21*, 694–700.

Fogg, V.C., Liu, C.J., and Margolis, B. (2005). Multiple regions of Crumbs3 are required for tight junction formation in MCF10A cells. J. Cell Sci. *118*, 2859–2869.

Goldstein, B., and Macara, I.G. (2007). The PAR proteins: fundamental players in animal cell polarization. Dev. Cell *13*, 609–622.

Grivennikov, S., and Karin, M. (2008). Autocrine IL-6 signaling: a key event in tumorigenesis? Cancer Cell *13*, 7–9.

Guarino, M., Rubino, B., and Ballabio, G. (2007). The role of epithelial-mesenchymal transition in cancer pathology. Pathology *39*, 305–318.

Győrffy, B., Lanczky, A., Eklund, A.C., Denkert, C., Budczies, J., Li, Q., and Szallasi, Z. (2010). An online survival analysis tool to rapidly assess the effect of 22,277 genes on breast cancer prognosis using microarray data of 1,809 patients. Breast Cancer Res. Treat. *123*, 725–731.

Hao, Y., Du, Q., Chen, X., Zheng, Z., Balsbaugh, J.L., Maitra, S., Shabanowitz, J., Hunt, D.F., and Macara, I.G. (2010). Par3 controls epithelial spindle orientation by aPKC-mediated phosphorylation of apical Pins. Curr. Biol. *20*, 1809–1818.

Harris, T.J., and Peifer, M. (2005). The positioning and segregation of apical cues during epithelial polarity establishment in *Drosophila*. J. Cell Biol. *170*, 813–823.

Horikoshi, Y., Suzuki, A., Yamanaka, T., Sasaki, K., Mizuno, K., Sawada, H., Yonemura, S., and Ohno, S. (2009). Interaction between PAR-3 and the aPKC-PAR-6 complex is indispensable for apical domain development of epithelial cells. J. Cell Sci. *122*, 1595–1606.

Hu, C., Diévart, A., Lupien, M., Calvo, E., Tremblay, G., and Jolicoeur, P. (2006). Overexpression of activated murine Notch1 and Notch3 in transgenic mice blocks mammary gland development and induces mammary tumors. Am. J. Pathol. *168*, 973–990.

Jansen, M., Ten Klooster, J.P., Offerhaus, G.J., and Clevers, H. (2009). LKB1 and AMPK family signaling: the intimate link between cell polarity and energy metabolism. Physiol. Rev. *89*, 777–798.

Januschke, J., and Gonzalez, C. (2008). *Drosophila* asymmetric division, polarity and cancer. Oncogene *27*, 6994–7002.

Kojima, Y., Akimoto, K., Nagashima, Y., Ishiguro, H., Shirai, S., Chishima, T., Ichikawa, Y., Ishikawa, T., Sasaki, T., Kubota, Y., et al. (2008). The overexpression and altered localization of the atypical protein kinase C lambda/iota in breast cancer correlates with the pathologic type of these tumors. Hum. Pathol. *39*, 824–831.

Litherland, G.J., Elias, M.S., Hui, W., Macdonald, C.D., Catterall, J.B., Barter, M.J., Farren, M.J., Jefferson, M., and Rowan, A.D. (2010). Protein kinase C isoforms zeta and iota mediate collagenase expression and cartilage destruction via STAT3- and ERK-dependent c-fos induction. J. Biol. Chem. *285*, 22414–22425.

Mazzone, M., Selfors, L.M., Albeck, J., Overholtzer, M., Sale, S., Carroll, D.L., Pandya, D., Lu, Y., Mills, G.B., Aster, J.C., et al. (2010). Dose-dependent induction of distinct phenotypic responses to Notch pathway activation in mammary epithelial cells. Proc. Natl. Acad. Sci. USA *107*, 5012–5017.

McCaffrey, L.M., and Macara, I.G. (2009). The Par3/aPKC interaction is essential for end bud remodeling and progenitor differentiation during mammary gland morphogenesis. Genes Dev. *23*, 1450–1460.

Pagliarini, R.A., and Xu, T. (2003). A genetic screen in *Drosophila* for metastatic behavior. Science *302*, 1227–1231.

Pearson, H.B., Perez-Mancera, P.A., Dow, L.E., Ryan, A., Tennstedt, P., Bogani, D., Elsum, I., Greenfield, A., Tuveson, D.A., Simon, R., and Humbert, P.O. (2011). SCRIB expression is deregulated in human prostate cancer, and its deficiency in mice promotes prostate neoplasia. J. Clin. Invest. *121*, 4257–4267.

Pece, S., Serresi, M., Santolini, E., Capra, M., Hulleman, E., Galimberti, V., Zurrida, S., Maisonneuve, P., Viale, G., and Di Fiore, P.P. (2004). Loss of

negative regulation by Numb over Notch is relevant to human breast carcinogenesis. J. Cell Biol. *167*, 215–221.

Ponzo, M.G., and Park, M. (2010). The Met receptor tyrosine kinase and basal breast cancer. Cell Cycle *9*, 1043–1050.

Qin, Y., Capaldo, C., Gumbiner, B.M., and Macara, I.G. (2005). The mammalian Scribble polarity protein regulates epithelial cell adhesion and migration through E-cadherin. J. Cell Biol. *171*, 1061–1071.

Ranger, J.J., Levy, D.E., Shahalizadeh, S., Hallett, M., and Muller, W.J. (2009). Identification of a Stat3-dependent transcriptional regulatory network involved in metastatic progression. Cancer Res. *69*, 6823–6830.

Raouf, A., Zhao, Y., To, K., Stingl, J., Delaney, A., Barbara, M., Iscove, N., Jones, S., McKinney, S., Emerman, J., et al. (2008). Transcriptome analysis of the normal human mammary cell commitment and differentiation process. Cell Stem Cell *3*, 109–118.

Reese, D.M., and Slamon, D.J. (1997). HER-2/neu signal transduction in human breast and ovarian cancer. Stem Cells *15*, 1–8.

Regala, R.P., Weems, C., Jamieson, L., Khoor, A., Edell, E.S., Lohse, C.M., and Fields, A.P. (2005). Atypical protein kinase C iota is an oncogene in human non-small cell lung cancer. Cancer Res. *65*, 8905–8911.

Rørth, P. (2009). Collective cell migration. Annu. Rev. Cell Dev. Biol. *25*, 407–429.

Rothenberg, S.M., Mohapatra, G., Rivera, M.N., Winokur, D., Greninger, P., Nitta, M., Sadow, P.M., Sooriyakumar, G., Brannigan, B.W., Ulman, M.J., et al. (2010). A genome-wide screen for microdeletions reveals disruption of polarity complex genes in diverse human cancers. Cancer Res. *70*, 2158–2164.

Schafer, Z.T., and Brugge, J.S. (2007). IL-6 involvement in epithelial cancers. J. Clin. Invest. *117*, 3660–3663.

Schmoranzer, J., Fawcett, J.P., Segura, M., Tan, S., Vallee, R.B., Pawson, T., and Gundersen, G.G. (2009). Par3 and dynein associate to regulate local microtubule dynamics and centrosome orientation during migration. Curr. Biol. *19*, 1065–1074.

Shackleton, M., Vaillant, F., Simpson, K.J., Stingl, J., Smyth, G.K., Asselin-Labat, M.L., Wu, L., Lindeman, G.J., and Visvader, J.E. (2006). Generation of a functional mammary gland from a single stem cell. Nature *439*, 84–88.

Song, Y., Qian, L., Song, S., Chen, L., Zhang, Y., Yuan, G., Zhang, H., Xia, Q., Hu, M., Yu, M., et al. (2008). Fra-1 and Stat3 synergistically regulate activation of human MMP-9 gene. Mol. Immunol. *45*, 137–143.

St Johnston, D., and Ahringer, J. (2010). Cell polarity in eggs and epithelia: parallels and diversity. Cell *141*, 757–774.

Thiery, J.P., Acloque, H., Huang, R.Y., and Nieto, M.A. (2009). Epithelial-mesenchymal transitions in development and disease. Cell *139*, 871–890.

Thompson, J.E., Cubbon, R.M., Cummings, R.T., Wicker, L.S., Frankshun, R., Cunningham, B.R., Cameron, P.M., Meinke, P.T., Liverton, N., Weng, Y., and DeMartino, J.A. (2002). Photochemical preparation of a pyridone containing tetracycle: a Jak protein kinase inhibitor. Bioorg. Med. Chem. Lett. *12*, 1219–1223.

Villadsen, R., Fridriksdottir, A.J., Rønnov-Jessen, L., Gudjonsson, T., Rank, F., LaBarge, M.A., Bissell, M.J., and Petersen, O.W. (2007). Evidence for a stem cell hierarchy in the adult human breast. J. Cell Biol. *177*, 87–101.

Viloria-Petit, A.M., David, L., Jia, J.Y., Erdemir, T., Bane, A.L., Pinnaduwage, D., Roncari, L., Narimatsu, M., Bose, R., Moffat, J., et al. (2009). A role for the TGFbeta-Par6 polarity pathway in breast cancer progression. Proc. Natl. Acad. Sci. USA *106*, 14028–14033.

Wu, M., Pastor-Pareja, J.C., and Xu, T. (2010). Interaction between Ras(V12) and scribbled clones induces tumour growth and invasion. Nature *463*, 545–548.

Xie, T.X., Wei, D., Liu, M., Gao, A.C., Ali-Osman, F., Sawaya, R., and Huang, S. (2004). Stat3 activation regulates the expression of matrix metalloproteinase-2 and tumor invasion and metastasis. Oncogene *23*, 3550–3560.

Yu, H., Pardoll, D., and Jove, R. (2009). STATs in cancer inflammation and immunity: a leading role for STAT3. Nat. Rev. Cancer *9*, 798–809.

Zen, K., Yasui, K., Gen, Y., Dohi, O., Wakabayashi, N., Mitsufuji, S., Itoh, Y., Zen, Y., Nakanuma, Y., Taniwaki, M., et al. (2009). Defective expression of polarity protein PAR-3 gene (PARD3) in esophageal squamous cell carcinoma. Oncogene *28*, 2910–2918.

Zhan, L., Rosenberg, A., Bergami, K.C., Yu, M., Xuan, Z., Jaffe, A.B., Allred, C., and Muthuswamy, S.K. (2008). Deregulation of scribble promotes mammary tumorigenesis and reveals a role for cell polarity in carcinoma. Cell *135*, 865–878.

Zhang, H., and Macara, I.G. (2006). The polarity protein PAR-3 and TIAM1 cooperate in dendritic spine morphogenesis. Nat. Cell Biol. *8*, 227–237.